Solid-density plasma nanochannel generated by a fast single ion in condensed matter

A. V. Lankin,[1,2] I. V. Morozov,[1,2] G. E. Norman,[1,2] S. A. Pikuz, Jr.,[1,2,*] and I. Yu. Skobelev[1]
[1]*Joint Institute for High Temperatures, RAS, 13 Bld. 2, Izhorskaya Street, Moscow, 125412, Russia*
[2]*Moscow Institute of Physics and Technology, 9 Institutskii pr., Dolgoprudny, 141700, Russia*
(Received 29 October 2008; published 30 March 2009)

A plasma model of relaxation of a medium in heavy-ion tracks in condensed matter is proposed. The model is based on three assumptions: the Maxwell distribution of plasma electrons, localization of plasma inside the track nanochannel, and constant values of the plasma electron density and temperature during the x-ray irradiation. The model of multiple ionization of target atoms by a fast projectile ion is used to determine the initial conditions. An analysis of the results of the calculations performed makes it possible to define when the atomic relaxation model is a very rough approximation and the plasma relaxation model must be used. It is demonstrated that the plasma relaxation model adequately describes the x-ray spectra observed upon interaction of a fast ion with condensed target. The comparison with the experimental data justifies the reliability of the plasma relaxation model. Preassumptions of plasma relaxation model are validated by the molecular-dynamics simulation. An x-ray spectral method based on the plasma relaxation model is proposed for diagnostics of the plasma in fast ion tracks. The results obtained can be useful in examining the initial stage of defect formation in solids under irradiation with single fast heavy ions.

DOI: 10.1103/PhysRevE.79.036407 PACS number(s): 52.27.Gr, 52.50.Gj, 52.65.Yy, 52.70.La

I. INTRODUCTION

The interaction of single fast heavy ion with condensed matter leads to the formation of a track. On the initial stage, the ion propagates through a matter and causes extensive ($\sim$100 μm) excited channel with transverse size of about 1 nm as it is illustrated in Fig. 1. This stage can be studied experimentally by measuring x-ray spectral lines generated by radiative decay of autoionized states of multiply charged ions of the target material. These ions appear due to the multiple ionization of the target atoms by the Coulomb field of a projectile ion. Some of the target atoms have vacancies in the K shell. As a result of radiative transitions from higher shells (L,M, etc.) to the K shell, the observed x-ray spectrum is emitted.

The simplest model to interpret x-ray spectra is based on the assumption that the relaxation of different ions is independent of each other as if these ions were isolated [1–4]. In this case, the intensity of the x-ray spectral line generated by the ion with spectroscopic symbol Z is proportional to the corresponding multiple-ionization cross sections multiplied by the branching factor $A^Z/(A^Z+\Gamma^Z)$, where A^Z is the radiative transition probability and Γ^Z is the autoionization probability. In what follows, we recall this model as an "atomic relaxation" one.

The atomic relaxation model relates the observed x-ray spectra only to the interaction of the projectile ion with individual target atoms, whereas the excited state of the target medium is not taken into account. In other words, the atomic relaxation model completely ignores the fact that the plasma-like environment arising after the initial ionization enables a wider range of relaxation processes for the excited ions. For example, owing to the collisions with free electrons, the initially excited Z ion can either be ionized or recombine before filling the K vacancy upon the radiative transition. It means that the initial excitation of the Z ion could actually result in the formation of ions with different charge states with K vacancies and, hence, could lead to the emission of spectral lines of ions with $Z' \neq Z$. In this case, the observed x-ray spectrum should reflect not only the characteristics of the interaction of the projectile ion with the target atoms but also the parameters (temperature and density) of the plasma formed.

The conclusion about the generation of plasma inside the track of a fast heavy ion was drawn quite long time ago [5–7]. Moreover, it was noted there that the plasma was strongly coupled (nonideal). Nevertheless only recently [8], the correspondence between the plasma parameters and the observed x-ray spectra was considered. It was done in the context of the so-called "plasma" relaxation model. This model is based on the solution of time-dependent equations of the radiative-collisional kinetics, while the initial state of

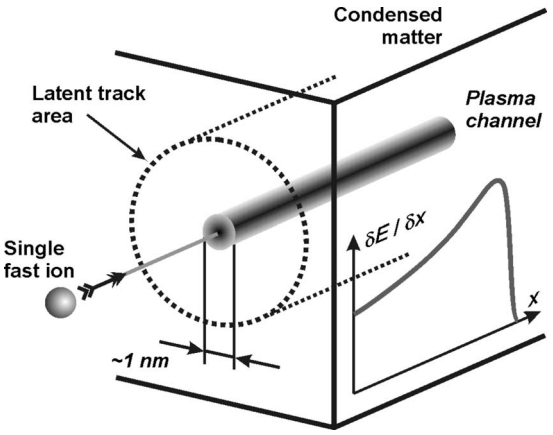

FIG. 1. Plasma channel created by single fast ion slowing down in condensed matter. The initial stage of channel relaxation can be investigated using x-ray radiation of multicharged target ions. Following relaxation leads to the formation of the latent ion track.

*Corresponding author; spikuz@gmail.com

the excited medium is described by the classical atomic relaxation model.

The atomic relaxation model has been used in a number of investigations (see, for example, [1–4,9–12]). Particularly, argon K_α x-ray satellites produced by ion collisions have been analyzed in high resolution [3]. The ions of H, C, N, O, F, Si, and Cl with energies in the range 1–5 MeV/amu were used to bombard Ar contained in a gas cell. It was the first systematic study of K_α x-ray satellites emitted from gaseous targets with $Z>10$. The relative satellite intensities and satellite energies were tabulated and their projectile dependence was qualitatively discussed. The average number of L-shell vacancies formed in single-K-vacancy-producing collisions was determined from a model calculation with theoretically obtained decay rates. It was also the first successful demonstration of the scaling law for multiple ionization by heavy ions with respect to the ion mass, charge, energy, and some other characteristics.

High-resolution measurements have been made for Ti K_α x-rays following bombardment of thick solid Ti targets by H^+, He^{n+}, Li^{n+}, C^{n+}, and O^{n+} ions with energies of 1–5 MeV/amu [9]. The measurements were accompanied with a systematic study of the influence of projectile atomic number Z_1 and energy on the relative intensities, centroid energies, and the widths of various x-ray peaks. It was shown that the satellite intensity increases with increasing Z_1 for the same-velocity projectile up to $Z_1=8$. It should be noted that the satellite intensities agreed roughly with predictions of the Coulomb-ionization theory modified to account for multiple ionization, except for the case of oxygen-ion projectiles where agreement with theory was rather poor. Authors [9] concluded that "more detailed studies of intensities, centroid energies, and peak widths are needed."

Such a detailed study is the main purpose of developing the plasma relaxation model in the present work. We discuss the area of applicability of the both atomic and plasma models. The material parameters, at which the plasma model changes over to the atomic relaxation model or at which the atomic relaxation model is too rough an approximation, are determined. Both models are used to interpret the measurements of x-ray spectra emitted during the interaction of Ni^{+14} ions with a SiO_2-aerogel target or Mg^{+7} ions with a solid Al target [13–16]. The ion beam energies under consideration are 3–11 MeV/amu; the density of SiO_2 aerogel are 0.15 g/cm^3.

The plasma relaxation model is formulated in Sec. II. The system of kinetic equations is presented in Sec. II A, and its solution is given for two different types of the initial conditions. Comparison with the atomic relaxation model is discussed. Sec. II B is devoted to the calculation of the x-ray spectra on the basis of the solution of the kinetic equations. The influence of the plasma environment is shown. The comparison with the experimental data in Sec. III justifies the reliability of the plasma relaxation model discussed above. This model is used for the diagnostics of the plasma temperature and ionization probability of inner electrons in Sec. IV. The model is based on three assumptions: the Maxwell distribution of plasma electrons, localization of plasma inside the track channel, and constant values of the plasma electron density and temperature during the x-ray irradiation. These assumptions are treated in Sec. V using molecular-dynamics (MD) simulations for the plasma parameters obtained in Sec. VI. Thus the self-consistency of the plasma relaxation model is proven.

II. PLASMA RELAXATION MODEL

A. Time-dependent kinetic equations and initial conditions

The plasma model of the target matter relaxation is based on (1) the conclusion of [5–7,17] that the solid-density nanosize plasma in the area of projectile-target atom interaction is created and on (2) the solution of the time-dependent equations of the collisional-radiative kinetics to describe the evolution of an initially created excited state. The initial target state is defined by the multiple ionization of target atoms by a projectile. We will consider further the solids consisted of atoms with nuclear charges ~10–18, i.e., having fully populated K and L shells and several electrons in M shell. Particularly, this is the cases of quartz and aluminum solid targets that have been investigated experimentally [13–16].

Initially, both free electrons and different multicharged ions with single K-shell vacancy, n L-shell vacancies, and fully ionized M shell are produced in the area of a single fast ion track. The populations N_n of the states with n vacancies in the L shell are proportional to the cross sections σ_n of the multiple ionization of the target atom by the field of the projectile ion. In the atomic relaxation model, the multiple-ionization cross section—as a rule (see, for example, [1–4,9])—is determined using the quasiclassical impact-parameter method. According to this method, the multiple-ionization cross section can be written in the form

$$\sigma_n = \sigma(1s)\frac{8!}{n!\,(8-n)!}p_L(0)^n[1-p_L(0)]^{(8-n)}, \qquad (1)$$

where $\sigma(1s)$ is the cross section of ionization of the $1s$ electron, $p_L(0)$ is the probability of ionization of the L electron at collision with the zero impact parameter, and n is the number of vacancies in the L shell of the ion created ($n=0$ for autoionizing states of fluorinelike ions, $n=1$ for autoionizing states of oxygenlike ions, etc.). The relationship (1) was derived under the assumption that the probabilities of the ionization of $2s$ and $2p$ electrons are equal. However, Eq. (1) can be easily extended to the case where these probabilities differ from each other. Let us designate the probabilities of the ionization of $2s$ and $2p$ electrons at the collision with the zero impact parameter as $p_{2s}(0)$ and $p_{2p}(0)$, respectively. Then, the generalized formula for the multiple-ionization cross sections can be represented in the form

$$\sigma_n = \sigma(1s)\sum_{k_1+k_2=n}\frac{2!}{k_1!\,(1-k_1)!}\frac{6!}{k_2!\,(8-k_2)!}p_{2s}(0)^{k_1} \times p_{2p}(0)^{k_2}[1-p_{2s}(0)]^{(2-k_1)}[1-p_{2p}(0)]^{(6-k_2)\sim}. \qquad (2)$$

Thus, in order to describe the initial conditions, it is sufficient to know the probabilities $p_{2s}(0)$ and $p_{2p}(0)$, which are the functions of the projectile ion charge, the target atom nuclear charge, and the projectile ion velocity. Unfortunately, the exact calculation of these quantities is a very complex problem. Furthermore, no published data are available on the

collisions of Ni^{14+} ions with the silicon atom or Mg^{7+} ions with the aluminum atom. Hence it will be assumed below that $p_{2s}(0)=p_{2p}(0)=p_L(0)$, where $p_L(0)$ is the first free parameter of our model.

The duration of the first stage of the plasma formation at each track point is actually determined by the time of the multiple ionization of the target atom and can be estimated as $\tau_1 \sim a/v$, where a is the atomic size and v is the projectile ion velocity. This duration varies in the range of $\tau_1 = 10^{-3}-10^{-2}$ fs for the experimental conditions considered.

Further evolution of excited states is described by the standard system of time-dependent kinetic equations (see, for example, [18]),

$$\frac{dN_k^Z}{dt} = \sum_{m,Z'} K_{km}^{ZZ'} N_m^{Z'}, \tag{3}$$

where $N_k^Z(t)$ is the k-state population of ions with the spectroscopic symbol Z and $K_{km}^{ZZ'}$ is the kinetic matrix depending on the plasma density and temperature. The off-diagonal elements of the matrix $K_{km}^{ZZ'}$ are the total probabilities of $(m,Z') \rightarrow (k,Z)$ transitions due to all elementary processes, while the diagonal elements are equal to the total decay probability of (k,Z) state with the opposite sign. As the relaxation of excited states occurs in plasma, it is necessary to take into account all processes occurring due to collisions of ions with free electrons, i.e., collisional excitation and deexcitation, collisional ionization, three-body and radiative recombination, dielectronic capture.

In most cases, the system of Eq. (3) is solved using the so-called quasistationary approximation [18], where the time derivatives for excited levels are assumed to be zero. It provides the solution only for ground states while the populations of excited states are determined from the solution of the substantially simpler system of algebraic equations. This method can be used when the relaxation rates of the excited levels are considerably higher than the relaxation rates of the ground states. The above approximation is not adequate in the case of solid-state plasma. Therefore, the system of Eq. (3) is solved for the ground and excited (autoionizing) ones states jointly in the present work.

We use the following assumptions, which made it possible to decrease the number of equations, thus essentially simplifying the problem. First, the system of Eq. (3) includes only ground configurations of the ions and their lowest-lying autoionizing configurations. Second, it is assumed that the populations of closely spaced levels of an ion are proportional to their total statistical weights. It is related to the fact that the probabilities of collisional transitions between these levels in a solid-state plasma exceed the probabilities of the radiative and autoionizing transitions. As a result, only one level (namely, $1s2l^{(n+m)}$) is introduced instead of the great number of terms related, for example, to the configurations $1s2s^n2p^{m(2S+1)}L_{(2J+1)}$. The simplified scheme of energy levels, for which the system of Eq. (3) has been solved, is shown in Fig. 2. The kinetic matrix accounts for the following processes in this case: the ionization by the ionization by an electron impact, three-body recombination, photorecombination, radiative decay, autoionization, and dielectron capture. It is believed that the plasma temperature and density, which determine the x-ray emission, remain unchanged in the course of relaxation processes. The values of atomic constants (such as the energies of electronic levels and the probabilities of radiative and autoionizing transitions) and the rates of collisional transitions are taken from [19,20].

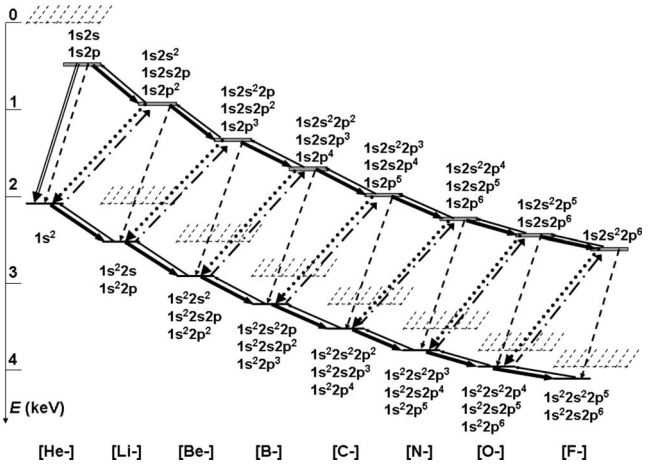

FIG. 2. The scheme of levels and atomic processes taking into account in the plasma model of track relaxation: radiative decay (dashed lines), autoionization (dotted line), dielectronic capture (dash-dotted lines), collisional ionization (thin solid lines), three-body recombination (thick solid lines), and collisional deexcitation (double solid line).

The expected temperatures of free electrons are within the range from 10 to 100 eV. The thermalization times for these electrons, as it will be shown in Sec. V C, do not exceed 1 fs. However, during the process of autoionization, electrons with considerably higher energies (1000–1400 eV) are created in the plasma as well. Since the thermalization times for these electrons may be longer than a few femtoseconds, which are important for the x-ray emission (cf. Sec. V C), it is necessary to consider the plasma with two fractions of electrons. During the initial ionization six to seven electrons per atom are produced and then each single autoionization act adds one more electron. It means that the fraction of hot free electrons is 13%–14% of the total electron number. While the Maxwell velocity distribution can be assumed for the low-temperature fraction of electrons, the high-temperature ones should have a rectangular distribution with the energies from 1100 to 1300 eV. This energy range corresponds to the electrons generated due to the autoionization of ions with different numbers of electrons in the L shell. In our case, the parameters of the high-temperature fraction of electrons are assumed to be fixed whereas the temperature T_e of the low-energy one is considered as the second free parameter of our model. It varies in the range of 10–300 eV. Therefore, all elementary collisional rates included into the system of Eq. (3) have been calculated for these two distribution functions of plasma electrons.

It should be noted that the above treatment is surely an approximate one because the electrons can move from one fraction to the other in the course of ionization and recombination. For example, an electron can either acquire a considerable energy due to the three-body recombination or lose

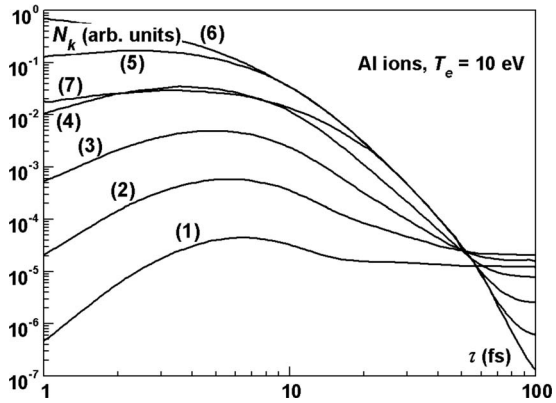

FIG. 3. The time dependences of autoionization states populations for Al ions at T_e=10 eV: F-like Al (1), O-like Al (2), N-like Al (3), C-like Al (4), B-like Al (5), Be-like Al (6), and Li-like Al (7). Be-like ion autoionization state was excited initially.

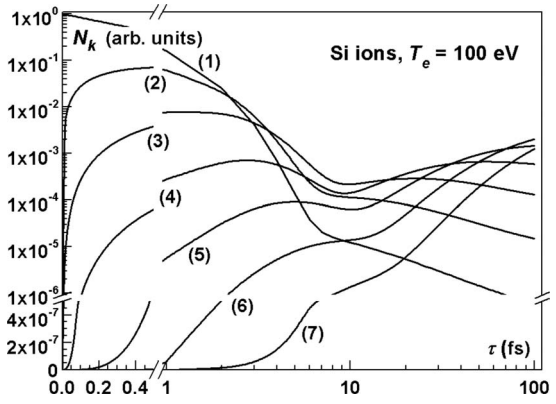

FIG. 4. Populations of Si ion autoionization states in dependence on time in plasma at T_e=100 eV: F-like Al (1), O-like Al (2), N-like Al (3), C-like Al (4), B-like Al (5), Be-like Al (6), and Li-like Al (7). F-like ion autoionization state was excited initially.

energy upon the ionization. Thus the aforementioned separation of electrons into two fractions is rather relative. However, this approach is physically justified in our case as it allows one to qualitatively distinguish between the first fraction which is predominantly responsible for the ionization of outer-shell electrons and the second one which is responsible for the dielectronic capture into autoionizing states and partially for the collisional ionization. From the other side, the numerical simulations [8] show that the role of high-energy fraction is rather small for the considered experimental conditions and its rough description does not influence significantly the spectra considered.

The solution of the system of Eq. (3) makes it possible to follow the relaxation of the initially generated state with the K vacancy in the Z_0 ion. The initial conditions have the form

$$N_k^Z(0) = N \text{ when } Z = Z_0, \quad N_k^Z(0) = 0 \text{ when } Z \neq Z_0, \quad (4)$$

where N is the atomic density of the target material. The examples of the calculation results are shown in Figs. 3 and 4, where the time dependences of the relative populations of autoinizing and ground levels are shown for silicon ions with the different charge states. Two types of the plasma nonequilibrium states are considered: plasma is recombining in Fig. 3 and plasma is ionizing in Fig. 4. The redistribution of the excitation among the different charge states turns out to be very significant in both cases. It justifies the importance of the plasma relaxation model.

B. X-ray spectra simulation

The solution of the system of Eq. (3) makes it possible also to calculate the emission spectrum observed during the passage of the heavy-ion flux through the condensed medium. In this case, the initial values of $N_k^Z(0)$ are proportional to the cross sections determined by Eq. (1). Let us introduce the total intensity I^Z of the array of the unresolved satellite transitions caused by the radiative decay of the autoionizing states of an ion with the spectroscopic symbol Z. It is emitted during the lifetime of the plasma τ_{plasma}. The values of I^Z are calculated from the formula

$$I^Z = \int_0^{\tau_{\text{plasma}}} N_k^Z(t) A_k^Z dt, \quad (5)$$

where A_k^Z is the probability of the radiative decay of the autoionizing state k.

As seen from Figs. 3 and 4, the establishment of equilibrium populations for the autoionizing states takes about 100 fs, but the relaxation for the most abundant ions is completed in 10–20 fs. Then the populations of their autoionizing states become relatively low. As the intensity of spectral line is proportional to the population of autoionizing states, the main contribution to x-ray radiation of plasma results from the times $t \leq 10-20$ fs, when the plasma is not only extremely nonequilibrium but also strongly nonstationary. Accordingly, the value of τ_{plasma}=20 fs is used in our spectra simulations.

Let us assume that the autoionizing state of ion Z is produced in the interaction of projectile ion with target atom. Then, in the frame of the atomic relaxation model, this ion can radiate with probability $A^Z/(A^Z+\Gamma^Z)$ x-ray photon with wavelength λ_Z. No other radiative process can take place.

Contrary to that in the plasma relaxation model, an initially produced ion can jump into any other ionization state Z' and radiate the photon with wavelength $\lambda_{Z'}$. The probability for this event can be determined from the solution of system (3). It depends on Z, Z', and on the plasma temperature (the plasma density is fixed in the model). The examples of calculation results are shown in Fig. 5.

The results of the plasma relaxation model differ fundamentally from the atomic ones. It is clearly seen in Fig. 5 that the relaxation of initially excited state in the ion Z stimulates the photon radiation by the ion $Z' \neq Z$ for any plasma temperature. For the high temperatures of T_e=100–300 eV, it takes place mainly for the ions with lower charges. For example [see Fig. 5(a)], the creation of an autoionizing state in F-like silicon ion can lead to the radiation of the satellite lines corresponding to the transitions in O-, N-, and C-like ions. At low plasma temperatures (T_e<50 eV), the above effect manifests itself primarily in the initially created autoionizing states of highly charged ions. For example [Fig.

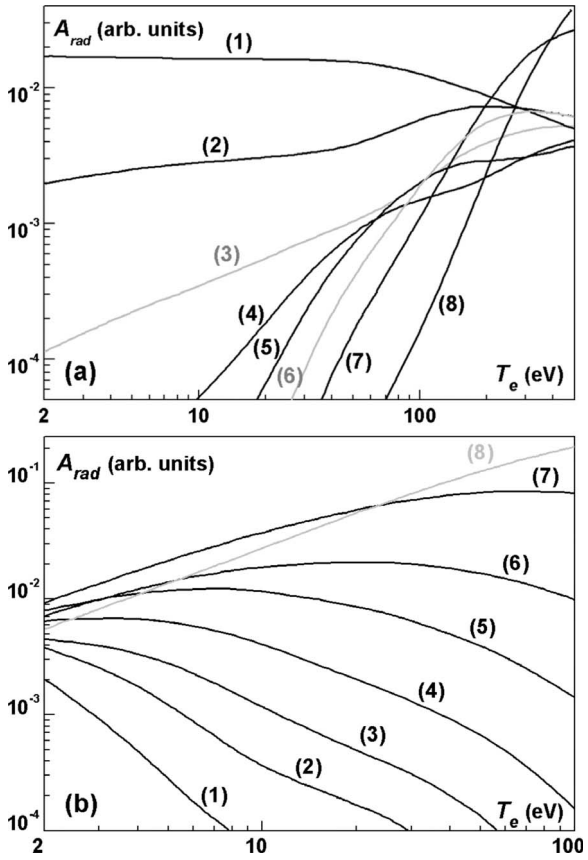

FIG. 5. Probability of x-ray photon radiation by Al ion in different charge states: F-like Al (1), O-like Al (2), N-like Al (3), C-like Al (4), B-like Al (5), Be-like Al (6), Li-like Al (7), and He-like Al (8). Autoionization state of F-like (a) or Li-like (b) ion was excited initially.

5(b)], the relaxation of the autoionizing state in the lithium-like silicon ion leads to the emission of satellite lines due to the transitions in the Be- and B-like ions.

It will be shown in Sec. III that the case of a low-temperature plasma is mostly interesting for diagnostic applications. The inelastic collisional processes, which are accompanied by the energy transfer from free electrons to the ions, are unimportant at low temperatures T_e. Equation (3) can be simplified substantially in this case to admit an analytic solution for the time-integrated intensities of the spectral transitions.

If we denote by the subscript k the autoionizing state of an ion with k vacancies in the L shell (e.g., $k=0$ corresponds to the $1s2s^22p^6$ autoionizing state in an F-like ion) then, for the intensities I_k of the spectral transitions due to the radiative decay of this autoionizing state, we obtain from Eq. (3) the following system of algebraic equations:

$$-N_i(0) = -\frac{\Gamma_i + A_i + N_e C_i^{dex} + N_e^2 C_{i,i-1}^{rc}}{A_i} I_i + \frac{N_e^2 C_{i+1,i}^{rc}}{A_{i+1}} I_{i+1}, \qquad (6)$$

where C_i^{dex} is the rate constant for the electron-impact deexcitation of the ith level and $C_{i,i-1}^{rc}$ is the rate constant for the three-body recombination from the ith level to the $(i-1)$th one.

The solution of Eq. (6) can be represented as

$$Ik = \sum_{j=k}^{N} I_{k,j}, \qquad (7)$$

where N is the state with the maximum energy and the contribution $I_{k,j}$ to the intensity of the kth line from the initially excited jth level is described by the expressions

$$I_{0,0} = N_0(0)\frac{A_0}{\Gamma_0 + A_0 + N_e C_0^{dex}},$$

$$I_{0,k} = N_k(0)\frac{\prod_{i=1}^{k} N_e^2 C_{i,i-1}^{rc}}{(\Gamma_0 + A_0 + N_e C_0^{dex})\prod_{i=1}^{k}(\Gamma_i + A_i + N_e C_i^{dex} + N_e^2 C_{i,i-1}^{rc})},$$

$$k > 0,$$

$$I_{k,k} = N_k(0)\frac{A_k}{\Gamma_k + A_k + N_e C_k^{dex} + N_e^2 C_{k,k-1}^{rc}}, \quad k > 0,$$

$$I_{j,k} = N_k(0)\frac{\prod_{i=j+1}^{k} N_e^2 C_{i,i-1}^{rc}}{\prod_{i=j}^{k}(\Gamma_i + A_i + N_e C_i^{dex} + N_e^2 C_{i,i-1}^{rc})},$$

$$\text{for } k > 0, \ 0 < j < k. \qquad (8)$$

A comparison of Eq. (8) with the numerical solution of Eq. (3) shows that formula (8) provides a satisfactory description of the line intensities in the range $T_e < 100$ eV.

III. COMPARISON WITH EXPERIMENTAL DATA

The results of the spectra simulation based on the plasma relaxation model can be compared with experimental data obtained recently in [14–16]. These experiments were carried out in the linear heavy-ion accelerator facility UNILAC (GSI, Darmstadt, Germany). Among other, the interaction of Ni^{+14} and Mg^{+7} fast ions with low (0.15 g/cm^3) bulk density quartz aerogel and solid Al targets has been investigated, correspondingly. Enough thickness of the target sample provided the full internal stopping of projectile ions. The use of the aerogel target allowed to expand the track length up to 2 mm, which provided the spatial resolution along the track for the spectra registered, Also it was shown in [13–15] that the inner nanoscale structure of aerogel did not influence stopping and media excitation processes in other respects.

The ions with the energy of 11.4 MeV/amu were focused into the 2 mm spot at the edge of a target. The target was exposed during 2–3 h by a beam current of 0.2–0.5 μA. Such a low current provided the average time interval of 10 ps between single-ion shoots. In this case, the probability for a next ion to propagate in the vicinity of the previous ion track during the track relaxation time was negligible. Thus the measured spectrum might be considered as an average

over the independent acts of a single heavy ion interaction with the cold target matter. The ion created the narrow plasma channel in each act. The x-ray spectra of the excited target matter were registered by means of the focusing spectrometers with spatial resolution (FSSR) based on the spherically bent crystal dispersion element. The spectral range 6.1–7.3 Å was embraced by use of the single quartz crystal ($2d$=8.512 Å) tuned on the first reflection order. It permitted to register simultaneously the dielectronic satellites of the He_α resonance line for every charge state of the Si target ion. The spectral range of 7.9–8.3 Å with the mica crystal ($2d$ =19.938 Å) working on the second reflection order covered the Al target emission spectra. The spectra were registered with one-dimensional (1D) spatial resolution along the direction of the projectile ion propagation.

The experimental data are time integrated [14–16]. Therefore the observed spectra represent the total radiation caused by the initial excitation of ions in the different charge states. Thus the spectra have to be described by Eq. (5), where the populations of the autoionizing states are given by the solution of kinetic equation system (3) with the initial conditions corresponding to Eq. (1).

It is necessary to consider the group of dielectronic satellite lines for every ion charge state. Such group consists of a number of radiation transitions (up to 40 for C-like Si ion), which are concentrated inside a narrow spectral range of about 0.05 Å. Since the spectral resolution in the experiments [14–16] does not exceed 3000, these transitions are unresolved and registered as a spectral peculiarity with the overall profile width defined by the distribution $g^Z A^Z(\lambda)$ rather than by broadening of individual lines. The spectral functions describing the shape for a group of unresolved transitions are taken from the experiments [14–16] and then approximated by Gaussian functions. For O-, N-, and C-like satellites, the sums of two Gaussians are used. The samples of the modeling spectra for different values of T_e are presented in Fig. 6. It is seen that the spectra are strongly temperature sensitive and consequently they can be used to determine the electron plasma temperature.

The modeling spectra are compared with those observed experimentally [14–16] for the interaction of projectile Ni^{+14} ions with the quartz aerogel target in Fig. 7. Three separate comparisons are given for spectra registered in three different points along the track corresponding to the mean projectile energy of 11, 6, and 3 MeV/amu. The electron density in the model is $N_e=4.5\times10^{23}$ cm^{-3} which corresponds to the mean charge $\langle Z\rangle=6.7$ of the target ions. Fitting the modeling spectra to the experimental ones by varying the parameter $p_L(0)$ and the electron plasma temperature T_e allows to determine these quantities in the different points of the ion track. Although only two fitting parameters are used, the experimental data and plasma model simulation results are in good agreement for all eight satellite groups, whereas even the best fit for the former atomic relaxation model fails to describe the experimental results [see Figs. 7(a)–7(c)].

Note that the modeling spectra differ from the experimental data for the spectral line with $\lambda=7.13$ Å. This line represents a set of the inner-shell transitions $2p$-$1s$ for every Si ion ranging from Si I (neutral K_α) to Si VI. However, the probability to produce simultaneously an ion with K-shell vacancy and with bound M-shell electrons is negligible low. It is well known that the δ electrons with energies of several keV are created in the track area due to the close collisions with projectile ions (see, for example, [21]). These electrons can excite the K_α line outside the track area as the free motion path for such electrons exceeds the track transversal dimensions by 1 order of magnitude [22]. Thus the observed spectral line 7.13 Å consists of K_α lines radiated by Si I and Si II ions outside the track overlapping with the dielectronic satellites radiated by F-like Si VI ions near the track axis. Naturally, its total intensity exceeds the intensity calculated for a single F-like satellite. Unfortunately, the available data for δ-electrons generation is still not enough to include this process into the model.

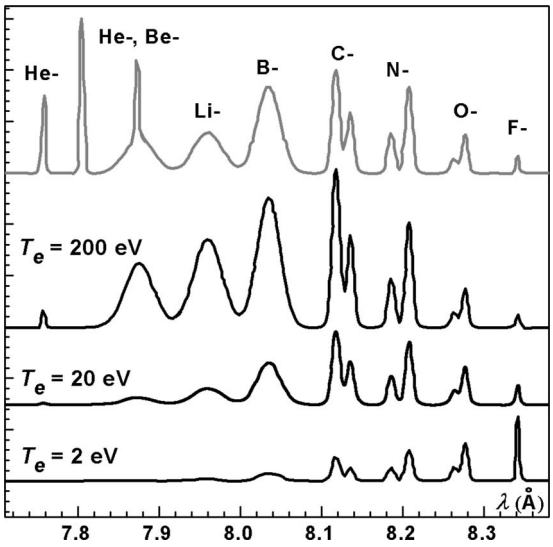

FIG. 6. The spectra of Al plasma radiation calculated according the plasma model of relaxation for $p_L(0)=0.34$ and different electron temperatures T_e: 2 eV, 20 eV, and 200 eV. The spectra simulation according the atomic model for $p_L(0)=0.34$ is shown on top as reference.

The calculated and experimental spectra [14–16] of solid Al target are compared in Fig. 8. The target was excited by single Mg^{+7} projectile ions with initial energies of 11 and 3 MeV/amu. The spectra calculations are done for the electron density of $N_e=4\times10^{23}$ cm^{-3}, which corresponds to the mean charge of the target ions $\langle Z\rangle=6.7$. One can see that the variation in two parameters $p_L(0)$ and T_e allows to achieve a good agreement between experimental and modeling data for all six satellite groups.

IV. PARAMETERS OF PLASMA NANOCHANNEL

The calculation results allow to define more accurately the phase of track relaxation that gives main contribution to the x-ray emission. The dependencies of the spectral line integral intensities (5) for Si VI–Si XIII ions on τ_{plasma} are shown in Fig. 9. These data are calculated for plasma parameters shown in Fig. 7(b). From Fig. 9, it can be concluded that the most intensive spectral lines are radiated predominately during the first 5–7 fs after the projectile ion has propagated. The plasma conditions at the later plasma relaxation stage

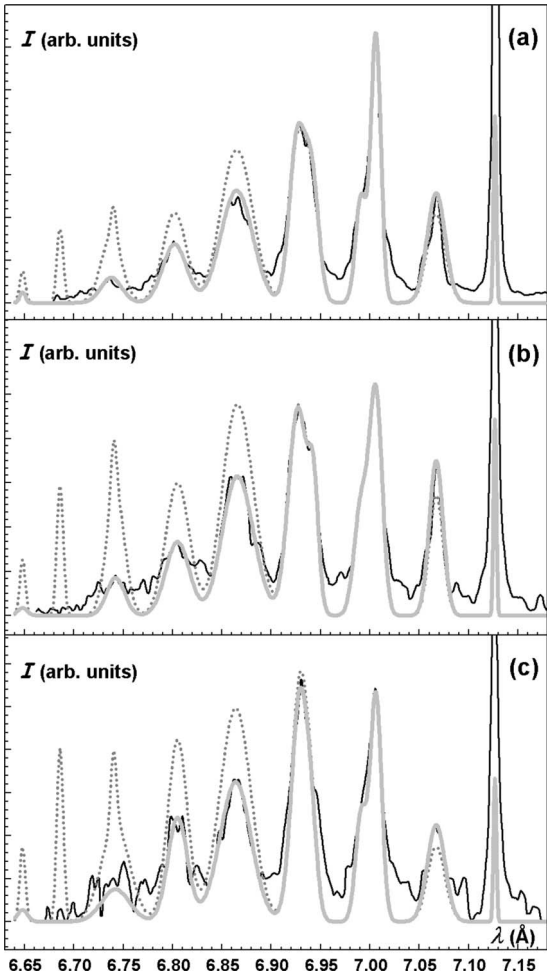

FIG. 7. Comparison of experimental spectra (thin solid lines) obtaining in [6–8] with modeling results. The spectra were radiated by Si ions inside aerogel SiO_2 target excited by Ni projectile ions with energy of 11 MeV/amu (a), 6 MeV/amu (b), and 3 MeV/amu (c). The modeling according the plasma model (thick solid lines) is done for (a) T_e=14 eV, $p_L(0)$=0.33; (b) T_e=15 eV, $p_L(0)$=0.335 and (c) T_e=25 eV, $p_L(0)$=0.34. For the atomic model simulation (dashed lines), the values of parameter (a) $p_L(0)$=0.335, (b) $p_L(0)$ =0.355, and (c) $p_L(0)$=0.375 were chosen.

($t \sim 10-20$ fs) may be important for the emission of low intensive lines only. Note that the x-ray spectra have been registered in the experiments [14–16] with no time resolution and with the moderate dynamic range. It means that the experimental spectrum is generally determined by the plasma radiation during the time interval 1–7 fs after excitation and carries the information about the media conditions in this stage of ion track relaxation.

It should be emphasized that the good agreement between the experimental and calculated intensities for the entire set of the spectral lines is achieved by variation in merely two free parameters $p_L(0)$ and T_e. It means that first the proposed plasma relaxation model is well appropriate and second the x-ray spectroscopy gives unique method to measure the plasma parameters inside the fast heavy-ion track. This method provides a tool for measuring not only the plasma temperature but also the probabilities $p_L(0)$ of L-shell elec-

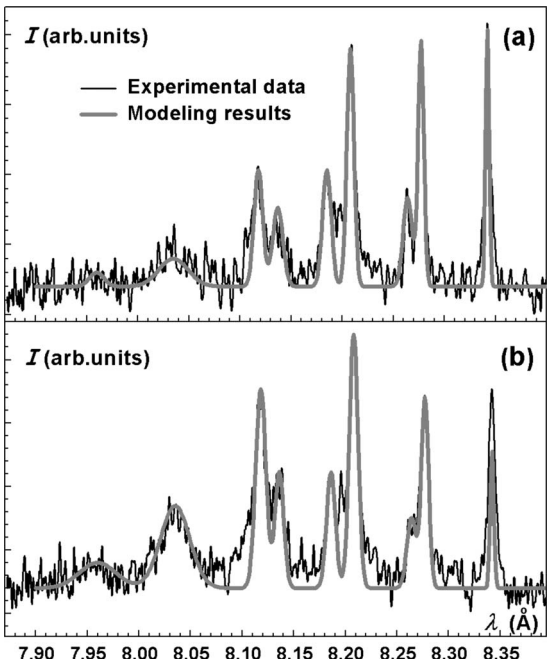

FIG. 8. Simulation according to the plasma model (thick lines) of experimental spectra [6–8] (thin lines) radiated by Al ions inside a track of Mg projectiles with energies of (a) 11 MeV/amu and (b) 3 MeV/amu. The modeling was done for (a) T_e=25 eV, $p_L(0)$=0.235 and (b) T_e=40 eV, $p_L(0)$=0.285.

tron ionization in collision with fast heavy ion for zero impact parameter.

Table I represents the values of $p_L(0)$ and T_e obtained by the simulation of the experimental data considered. As seen, the value of $p_L(0)$ depends very weakly on the projectile ion energy in the range of $E \sim 3-11$ MeV/amu. The values of $p_L(0)$ and their energy dependence for the interaction of Ni^{+14} ions with Si targets have not been described before.

In contrast to $p_L(0)$, the plasma temperature increases significantly with projectile ion slowing down to

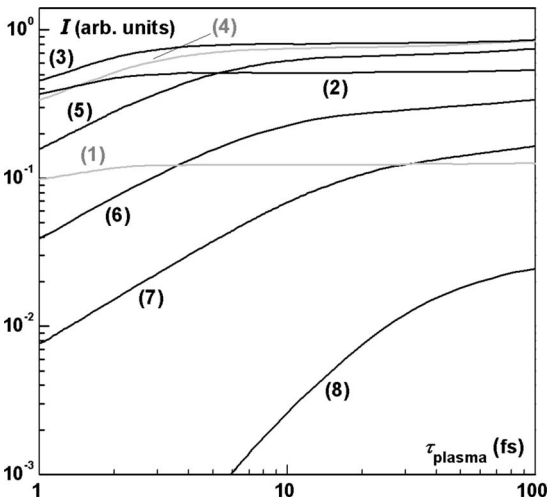

FIG. 9. Intensity of dielectronic satellites spectral lines radiated by Al ions in different charge states in dependence on plasma lifetime. The data is calculated by use of plasma model for T_e=40 eV and $p_L(0)$=0.285.

TABLE I. The plasma parameters were determined from spectra simulation according to the plasma model for the experimental conditions and data obtained in [6–8].

			Measured parameters				
Projectile target	Projectile energy (MeV/amu)	Electron density (10^{23} cm^{-3})	$p_L(0)$	T_e (eV)	N_D	Γ	θ
Ni^{+14}-SiO_2	11	4.5	0.33	14	0.13	1.3	0.18
Ni^{+14}-SiO_2	6	4.5	0.335	15	0.15	1.2	0.16
Ni^{+14}-SiO_2	3	4.5	0.34	25	0.32	0.71	0.076
Mg^{+7}-Al	11	4.0	0.235	25	0.34	0.68	0.067
Mg^{+7}-Al	3	4.0	0.285	40	0.69	0.43	0.033

$E \sim 3$ MeV/amu. The latter reflects the fact that the linear energy loss of the projectile ion is increasing along with the stopping process from 11 to 3 MeV/amu [16,23].

The last three columns in Table I contain the values of the electron-electron nonideality parameter $\Gamma = (4\pi n_e/3)^{1/3} e^2/(k_B T_e)$, the formal number of electrons in the Debye sphere $N_D = 4\pi r_D^3 n_e/3$, $r_D = \sqrt{k_B T/4\pi n_e e^2}$, and the degeneracy parameter $\theta = N_e(\hbar^2/mT_e)^{3/2}$. The values of the plasma parameters obtained show that plasma turns out to be strongly coupled and nondegenerate.

V. PLASMA MODEL VALIDATION

The main feature of the proposed plasma model is that it accounts not only for the collisionless relaxation of the initially generated autoionized ions (by means of further autoionization and radiative decay) but also for the relaxation caused by electron-ion collisions in the surrounding dense plasma. A number of assumptions are implicitly used at the formulation of the plasma relaxation model. The rates of the collision transition used at the solution of Eq. (3) are calculated for the Maxwell distribution of plasma electrons. Then the plasma parameters are considered to be time-independent in Eq. (3). It means that both plasma nanochannel and three-electron recombination of plasma electrons with ground-state ions should be negligible during the period of x-ray emission. It is necessary to prove the validity of these assumptions for the plasma parameters obtained in Sec. IV in order that our plasma relaxation model could be considered as a self-consistent one.

The first assumption is related to the calculation of the equilibration time for the electron velocity distribution function. As to the second one, the initial plasma density is known from the deposited energy but it can be decreased due to the diffusion of electrons out of the track area and due to the recombination of free electrons to the high-energy bound states. The rates of equilibration, diffusion, and recombination of electrons can be obtained by means of numerical simulations.

A. Simulation technique

As seen from Table I, the electron gas is nondegenerate and essentially strongly coupled. Relaxation processes in such plasma can be studied by the nonequilibrium MD simulations [24]. At the first stage, the electrons are equilibrated using the periodical boundary conditions with the given plasma parameters n_e and T_e which correspond to the state after ionization by the projectile. In order to simulate relaxation inside the plasma cylinder with a free surface, the periodical boundaries are canceled for X and Y axes. Thus the electrons were able to spread in X-Y plane. The final results are obtained averaging over 200–1000 relaxation processes. Each process started from statistically independent but macroscopically identical initial state [25].

The initial structure of ions in the cylinder cross section is shown in the inset in Fig. 10. Six ions with charge $Z=2$ are located at apexes of the hexahedron and the seventh one with $Z=4$ is in the center of the cell. The cell is periodically extended along the Z axis with the period a equals to the edge of hexahedron. Although this is a relatively rough approach to the real ion structure in SiO_2, it is appropriate to estimating the required relaxation times.

B. Relaxation of free electron velocities

First, let us consider the relaxation of the electron velocity distribution function. Simulations start from an artificially prepared initial state where all electrons have the same absolute value of the velocity equals to $v_{th} = (3k_B T_e/m_e)^{1/2}$ with

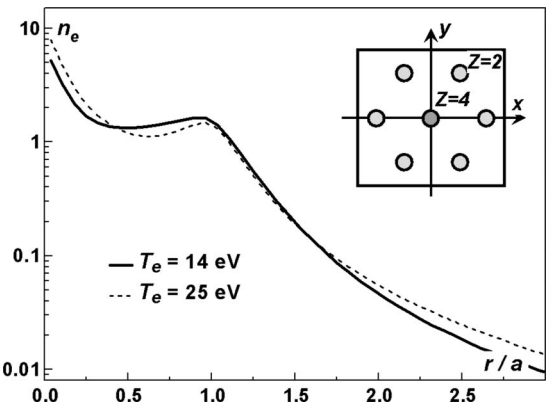

FIG. 10. Steady-state radial profile of the electron number density in the electric double layer. The distance from the track axis r is in units of the interatomic distance a. The temperatures of electrons are $T_e=14$ eV (solid curve) and $T_e=25$ eV (dashed curve). The arrangement of ions in the track cross section is given in the inset.

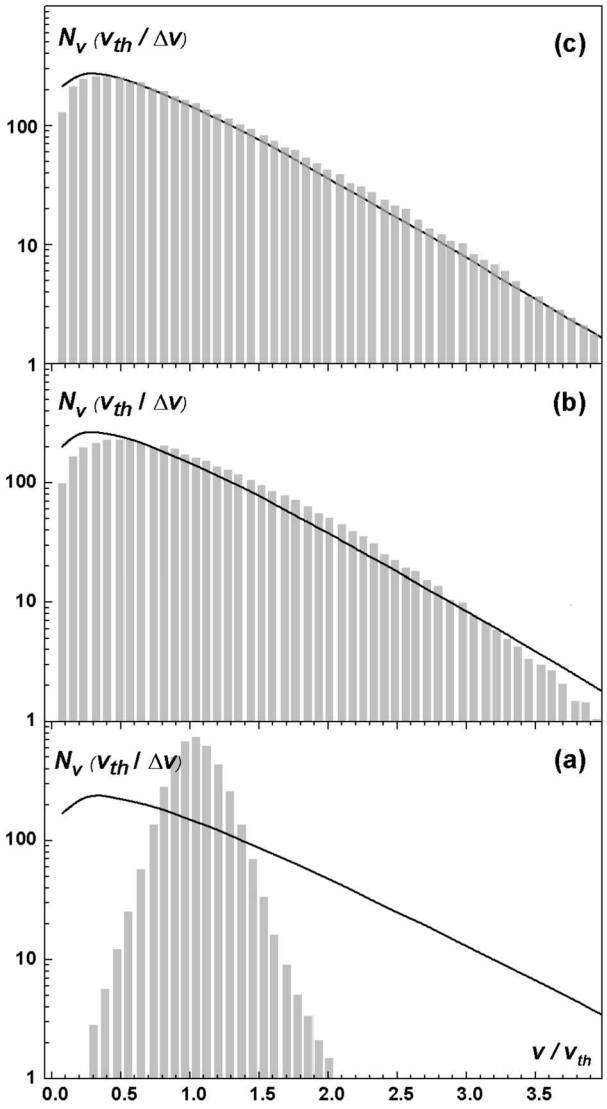

FIG. 11. Distribution of free electron velocities normalized by thermal velocity $v_{\mathrm{th}}=(3k_BT/m)^{1/2}$ with $T_e=14$ eV at the consecutive moments of time: (a) 0.005 fs, (b) 0.05 fs, and (c) 0.3 fs. The initial distribution is $f(v)=\delta(v\text{-}v_{\mathrm{th},0})$. The solid line indicates the Maxwell distribution for $T_e=3E_k/2k_B$, where E_k is a mean kinetic energy of electrons; Δv is the distribution step.

$T_e=14$ eV. Direction of the velocities is random. The relaxation of such distribution to the equilibrium one is shown in Fig. 11. Only electrons inside the cylinder $r<1.5a$ were taken into account. As seen from Fig. 4(b), the distribution is close to the Maxwell one at $t=0.05$ fs, but the exponential slope is not related to the correct value of the mean kinetic energy. Finally at $t=0.33$ fs, the distribution fits perfectly the equilibrium one for the considered velocity range. This value can be taken as the equilibration time for the electron velocity distribution function. For $T_e=25$ eV, the relaxation time is $t=0.25$ fs. As these times are lower than the time of x-ray spectra irradiation by 1 order of magnitude, one can assume that the plasma is in equilibrium during the whole time of the ion relaxation.

Generally speaking, the applicability of this approach depends neither on plasma degeneracy nor on the nonideality.

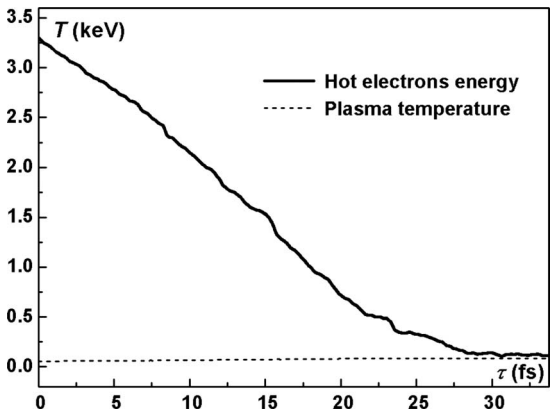

FIG. 12. Relaxation of the mean kinetic energy of a fraction of "fast electrons" which have the initial energy correspondent to $T_b(0)=3.3$ keV (solid curve). Dashed line shows the temperature of the bulk plasma.

However in this work, the relaxation kinetics (3) was calculated for the ideal classical plasma, i.e., collisional relaxation rates implied the Maxwell distribution of free electrons and the three-particle recombination rate was taken without nonideality corrections. At relatively high electron temperatures (in fact for $T_e>20$ eV), this assumption is quite reasonable. Although the particular values of the kinetic coefficients can be different for other sorts of plasma, the general statement about the role of collisional processes remains the same.

Coming back to the question of applicability of the Boltzmann statistics, one should note that for $T_e=14-15$ eV the degeneracy parameter $\theta=0.16-0.18$ which may slightly change the energy distribution of electrons toward the Fermi one. Qualitatively it means that for the same temperature, the mean electron energy increases. In particular, it leads to the overestimation of the three-body recombination rate (which is the predominant recombination process at such temperature) by using the Boltzmann statistics.

Let us now consider the relaxation of a small part of high-energy electrons with $T_b\approx 3$ keV. The equilibration process for such electrons is shown in Fig. 12. As the density of the high-energy electrons is 1000 times lower than the density of the bulk plasma, they do not affect the overall temperature. It is seen from the figure that the equilibration time is about 30 fs, which is greater that the time of the x-ray spectra irradiation. Thus this fraction of electrons should be treated separately when solving the kinetic equations for ions.

C. Relaxation of the spatial distribution

The next question is the decrease in free-electron density due to the diffusion from the central track area. As the plasma is neutral in large, spreading of the electron cloud produces positive charge in the track center and double electric layer on the track surface. The ion motion can be neglected when studying the dynamics of electrons. The stable radial density profiles of electrons obtained by MD simulations for two cases of $T_e=25$ eV and $T_e=14$ eV are shown in Fig. 10. The first peak at $r=a$ corresponds to the outer ion shell.

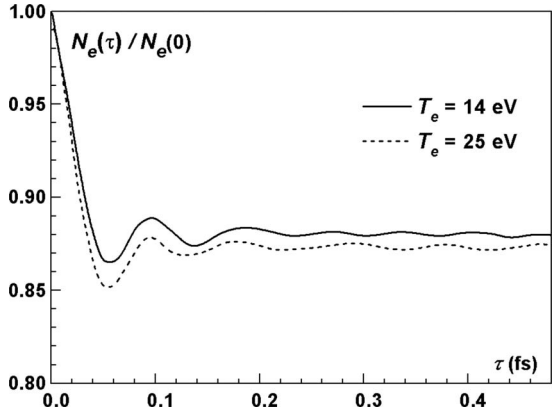

FIG. 13. Evolution of the total number of electrons inside the cylinder $r<1.5a$ related to the initial value; $T_e=14$ eV (solid curve) and $T_e=25$ eV (dashed curve).

The equilibration process for these distributions is shown in Fig. 13. For both values of the temperature, the equilibration time turned out to be about 0.5 fs. From the figure, it follows that the number of electrons remaining in area $r<1.5a$ decreases not more than below 85% of initial density. These electrons form the plasma around radiating ions which is dense enough for the collisional relaxation of ions. Another simulation which accounts for the nonzero permittivity of the surrounding media ($\varepsilon=2.25$) results in similar values.

It should be noted that approaching to the stable distribution for electrons is accompanied by oscillations of the plasma surface. Although, the detailed discussion on this phenomenon is out of the scope of this work.

D. Three-body recombination with autoionizing state ions

As the plasma in the track core is substantially strongly coupled and contains highly charged ions, the rate of collisional recombination used in Sec. II could differ from that for the three-body recombination in an ideal plasma. The effect of nonideality on the three-body recombination in the presence of multicharged ions is considered in [26]. According to [26], this effect becomes significant when

$$(4\pi/3)(0.78Ze^2/T_e)^3N_i=2(\Gamma_{Ze})^3\geq 1, \tag{9}$$

where $\Gamma_{Ze}=Ze^2N_i^{1/3}/T_e$ is the electron-ion nonideality parameter, N_i is the density of recombining ions. The main recombination process influenced on autoionizing level populations is the three-body recombination of the ions in low-populated autoionization states (see Fig. 2),

$$1s2l^m+e+e\rightarrow 1s2l^{(m+1)}+e. \tag{10}$$

Taking into account only the density of $1s2l^{(m+1)}$ ions, we obtained the value $2(\Gamma_{Ze})^3\ll 1$, so the nonideality effects are negligible. It means that nonideality effects have no influence on the intensities of dielectronic satellite transitions.

E. Collisional recombination with the ground-state ions

Another recombination process involves ions in ground state. In ideal plasma, it looks as

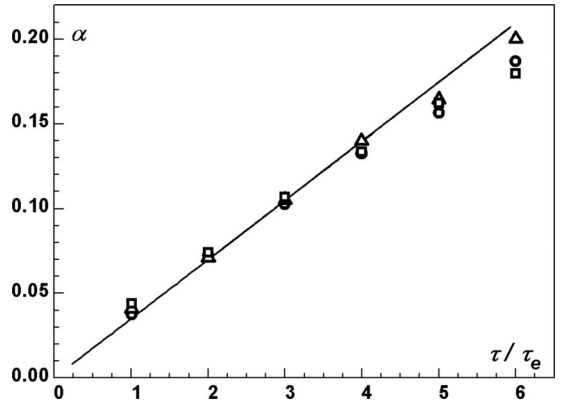

FIG. 14. The part of bound pairs α during the initial relaxation of the matter with potential depth of 5 kT (triangles), 10 kT (circles), and 15 kT (rectangles). Solid line corresponds to $\Gamma=1$.

$$1s^22l^m+e+e\rightarrow 1s^22l^{(m+1)}+e, \tag{11}$$

Attempts to include nonideality effects in the process (11) are done in [26–35]. All the approaches point to the suppression of the recombination. However, they are based on essential approximations, their results do not agree with each other, and there are no reliable expressions to calculate the recombination rate in strongly coupled plasmas (SCP).

Contrary to the ideal plasmas, the recombination with the ground-state ions in SCP can hardly be reduced to the three-body process. Therefore, we use the term collisional recombination for this process. Collisional recombination reduces to the three-body recombination at the decrease in nonideality. We use the fluctuation approach and MD modeling and simulation (see [36,37] for details) to study the process of the collisional recombination in SCP and to obtain the rate of the process for a certain range of nonidealities and a number of ion charges. This rate is related to the rate of the formation of the bound electron-ion pairs which appear as pair fluctuations in equilibrium plasma. Such pairs can be studied by MD simulations with the electron-ion interaction potentials in the form of the Coulomb one with a cutoff at $E=-3kT_e$.

The following numerical algorithm [36] is used. It consists of two parts. The first part is preliminary: a certain procedure of excluding pairs from the equilibrium plasma is repeated several times to create an initial state without pair fluctuation. The second part is the main one: the initial state created is used to start the relaxation MD run and to define the initial rate of the pair appearance according to the expression,

$$K=d\alpha/dt|_{\tau=0}, \tag{12}$$

where α is the fraction of pairs in the system, K is the frequency of pair production or the collisional recombination rate. The simulations are made for different values of the potential depth and nonideality parameter. As seen from Fig. 14, the recombination rate is generally independent of the potential depth. It means that the free electrons recombine first to weakly bound pairs (pair fluctuations) and only then to the low-lying atomic energy levels.

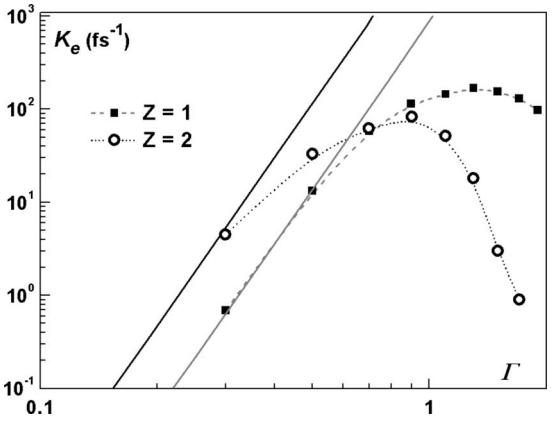

FIG. 15. The dependence of recombination rate on plasma nonideality for $T_e=15$ eV and different ion charge Z. Solid lines correspond to the three-body recombination rate in ideal plasma.

The dependence of recombination rate on plasma nonideality (Fig. 15) has a maximum at $\Gamma \sim 0.9$. In weakly coupled case, the calculation results are in good agreement with the known result for the three-body recombination rate in ideal plasmas,

$$K = Ce^{10}Z^3m^{-1/2}nT^{-9/2}, \tag{13}$$

where $C=1-3$ [38,39]. For higher nonideality, the recombination rate turns out to be considerably smaller then expected from Eq. (13) and decreases with the nonideality parameter growth. In Fig. 15, the recombination rates for the cases of singly and doubly charged ions are compared. Both curves have the similar shape but their peaks do not coincide. If the nonideality is weak ($\Gamma<0.7$), the recombination for doubly charged ions is faster and vice versa. The difference between these two curves grows monotonously with the plasma nonideality. In the limit of the ideal plasma, they both approach Eq. (13).

The recombination rate depends also on the ion dynamics in the plasma. Simulation results show (Fig. 16) that the recombination rate is higher in the case of movable ions compared to the case of fixed ionic lattice. The relative difference is greater than by a factor 2 for $\Gamma<1.4$ and vanishes with the nonideality growth. This result implies that the ion density fluctuations may play a role in the formation of electron-ion bound pairs. As the distance between ions in the case of doubly charged ions is larger for the same electron density, the considered effect disappears at a lower value of plasma nonideality ($\Gamma<0.7$). Another reason for that is the self-ordering of movable ions where the interaction between ions dominates. The role of self-ordering grows with the increase in ion charge.

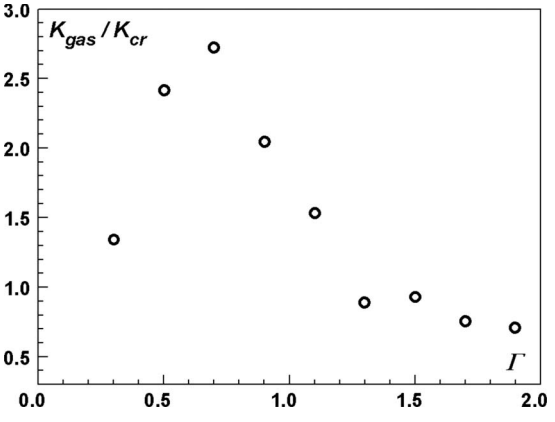

FIG. 16. The relation between the recombination rate for gaslike plasma and for ions fixed in crystal lattice points ($Z=1$) in dependence on plasma nonideality.

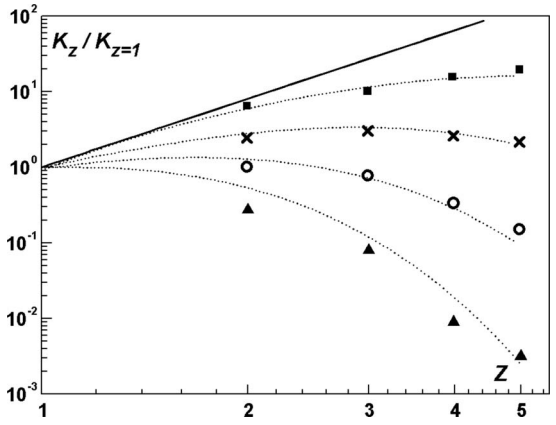

FIG. 17. Recombination rate in dependence on ion charge Z for different plasma nonideality: $\Gamma=0.3$ (rectangles); $\Gamma=0.5$ (crosses); $\Gamma=0.7$ (circles); and $\Gamma=0.9$ (triangles). Solid line corresponds to the ideal plasma.

It should be noted that the nonideality effect on recombination is stronger for the plasma with highly charged ions. As an example, the recombination rate differs noticeably from that one for an ideal plasma even for $\Gamma \sim 0.3$. In general, the obtained recombination rate is below the extrapolation of ideal plasma theory and this difference grows with the increase in both the plasma nonideality and the ion charge (Fig. 17).

Let us come back to the SCP created in the track nanochannel. Using the plasma temperature $T_e=25$ eV, the mean ion charge $Z=6$, and the nonideality parameter $\Gamma=0.7$, one can estimate the recombination time which gives 17 ps. It exceeds the period of measured x-ray radiation by orders of magnitude. Therefore the suggesting plasma model of track relaxation is applicable to describe a track area with $T_e \geq 20$ eV. For lower temperatures, the model describes properly the relaxation of autoionization states and the radiation of x-ray spectra, but it could underestimate the relaxation time for the ion charge distribution. Correct description of the ground-state population and its evolution at lower temperatures requires taking into account the degeneracy of electrons.

Using the determined plasma temperature, the estimation on transversal dimension of plasma channel can be asserted. If one assumes that the whole energy of a projectile ion is transferred to the ionization of the target atoms, the estimation for the plasma channel diameter gives ~ 3 Å. This value exceeds sufficiently both the Debye radius and the mean distance between electrons.

Generally, the considered plasma object resembles the one created in solid and gas cluster targets by intense femtosec-

ond laser pulses (see, for example, [40–42]). The principal distinction is that in our case, the initial distribution of ion excitation states is determined by a single impact of the charged projectile particle not by free electrons heated with a laser pulse. The lifetimes of plasmas created by intense laser pulses and fast heavy ion could differ from each other by orders of magnitude.

VI. CONCLUSION

The plasma relaxation model is considered to describe the excitation of solids by single fast ions with total energies of 0.1–1.0 GeV. Three time stages of the formation of a nonequilibrium strongly coupled solid-state nanoplasma are studied in the region of the track.

The state of the medium is described by the conventional atomic relaxation model at the initial stage ($\sim 10^{-2}$ fs). The initial channel of ionized matter is produced with the transversal diameter of several nanometers and electron density of $n_e \sim 10^{23}$ cm^{-3} ($Z=2-6$). Ions with K-shell vacancies are localized in the vicinity of the channel axis. Although their fraction is relatively low, they are responsible for the appearance of x-ray emission spectra.

Maxwell distribution of free electrons is established at the second stage (≤ 1 fs) with the temperature of tens of eV. The electric double layer with thickness of about interatomic distance is formed around the nanoscale initial channel. Further evolution (tens of femtosecond) of initially created charge state distribution for the ions with i-shell vacancies is described by the time-dependent equations of collisional-radiation kinetics. The ions are stable in the crystal lattice so that the band structure is not disrupted (though it is changed) while the matter is still deeply ionized.

X-ray K-shell spectra of solid quartz and Al targets excited by 100–600 MeV single ions [14–16] are explained with a good agreement between the proposed model simulation and the experimental data. Both the agreement and molecular-dynamics modeling confirm the validity and self-consistency of the plasma relaxation model. For the experimental conditions, the electron density and temperature are found to be equal to 4×10^{23} cm^{-3} and 10–50 eV, respectively. Thus the number of electrons in the Debye sphere is in the range of 0.14–0.32. So the plasma is strongly coupled.

The x-ray spectroscopy method is proposed to measure the plasma temperature in the fast multicharged ion track.

The obtained results can be used to study the further stages of heavy-ion track evolution: the melting of overheated ionic lattice in the presence of hot electrons, two-temperature hydrodynamics of track expansion, shock wave propagation, recombination, cooling, the formation of a latent track (for example, the defect formation under neutron irradiation is considered in [43,44]), and finally a change in the properties of the material with accumulation of tracks.

ACKNOWLEDGMENTS

The authors appreciate B. Doyle, H. Hjalmarson, J. Aidun, M. M. Basko, B. M. Smirnov, V. S. Vorobyev, and A.Ya. Faenov for prolific discussions and valuable suggestions. The work was partly supported by RFBR under Grant No. 07-08-00738-a, by RF President under Grant No. MK-4375.2008.8, and by Program of fundamental research No. 12 of the Presidium of RAS. S.A.P. and I.V.M acknowledge CRDF BRHE program. I.V.M. and A.V.L. acknowledge the "Dynasty" foundation. Simulations were performed on MIPT-60 cluster.

[1] R. L. Kauffman, J. H. McGuire, P. Richard, and C. F. Moore, Phys. Rev. A **8**, 1233 (1973).
[2] R. L. Kauffman, C. W. Woods, K. A. Jamison, and P. Richard, Phys. Rev. A **11**, 872 (1975).
[3] C. Schmiedekamp, B. L. Doyle, T. J. Gray, R. K. Gardner, K. A. Jamison, and P. Richard, Phys. Rev. A **18**, 1892 (1978).
[4] Y. Awaya, T. Kambara, and Y. Kanai, Int. J. Mass Spectrom. **192**, 49 (1999).
[5] R. H. Ritchie and C. Claussen, Nucl. Instrum. Methods Phys. Res. **198**, 133 (1982).
[6] A. M. Miterev, Khim. Vys. Energ. **21**, 332 (1987).
[7] E. G. Gamaly and L. T. Chadderton, Proc. R. Soc. London, Ser. A **449**, 381 (1995).
[8] A. V. Lankin, I. V. Morozov, G. E. Norman, and I. Yu. Skobelev, Zh. Eksp. Teor. Fiz. **133**, 701 (2008); [JETP **106**, 608 (2008)].
[9] K. W. Hill, B. L. Doyle, S. M. Shafroth, D. H. Madison, and R. D. Deslattes, Phys. Rev. A **13**, 1334 (1976).
[10] B. L. Doyle, U. Schiebel, J. R. Macdonald, and L. D. Ellsworth, Phys. Rev. A **17**, 523 (1978).
[11] A. Schmiedekamp, T. J. Gray, B. L. Doyle, and U. Schiebel, Phys. Rev. A **19**, 2167 (1979).
[12] B. L. Doyle and D. K. Brice, Phys. Rev. A **24**, 2232 (1981).
[13] O. N. Rosmej *et al.*, Rev. Sci. Instrum. **74**, 5039 (2003).
[14] O. N. Rosmej *et al.*, Phys. Rev. A **72**, 052901 (2005).
[15] O. N. Rosmej *et al.*, Laser Part. Beams **23**, 1 (2005).
[16] S. A. Pikuz, Jr., V. P. Efremov, O. Rosmej, A. Blazevic, S. Korostiy, A. Fertman, A. V. Shutov, G. E. Norman, and D. H. H. Hoffmann, J. Phys. A **39**, 4765 (2006).
[17] A. M. Miterev, Usp. Fiz. Nauk **172**, 1131 (2002); [Phys. Usp. **45**, 1019 (2002)].
[18] L. M. Biberman, V. S. Vorobyev, and I. T. Yakubov, *Kinetics of Nonequilibrium Low-Temperature Plasmas* (Springer, Berlin, 1987).
[19] L. A. Vaynshtein, I. I. Sobelman, and E. A. Yukov, *Atom Excitation and Spectral Line Broadening* (Nauka, Moscow, 1979).
[20] A. Ya. Faenov, S. A. Pikuz, and A. S. Shlyaptseva, Phys. Scr. **49**, 41 (1994).
[21] G. Schiwietz, J. P. Biersack, D. Schneider, N. Stolterfoht, D. Fink, V. J. Montemayor, and B. Skogvall, Phys. Rev. B **41**, 6262 (1990).
[22] H. Schmidt-Böcking, J. P. Biersack, D. Schneider, N. Stolterfoht, D. Fink, V. J. Montemayor, and B. Skogvall, Adv. Space

Res. **12**, 7 (1992).
[23] J. F. Ziegler, Nucl. Instrum. Methods Phys. Res. B **219-220**, 1027 (2004).
[24] I. V. Morozov and G. E. Norman, Zh. Eksp. Teor. Fiz. **127**, 412 (2005); [JETP **100**, 370 (2005)].
[25] A. Yu. Kuksin, I. V. Morozov, G. E. Norman, V. V. Stegailov, and I. A. Valuev, Mol. Simul. **31**, 1005 (2005).
[26] L. M. Biberman, V. S. Vorobyev, and I. T. Yakubov, Dokl. Akad. Nauk SSSR **296**, 576 (1987); [Sov. Phys. Dokl. **32**, 752 (1987)].
[27] Yu. K. Kurilenkov, Teplofiz. Vys. Temp. **18**, 1312 (1980).
[28] M. Schlanges and Th. Bornath, Physica A **192**, 262 (1993).
[29] Th. Bornath and M. Schlanges, Physica A **196**, 427 (1993).
[30] Y. Hahn, Phys. Lett. A **231**, 82 (1997).
[31] Y. Hahn, Phys. Lett. A **293**, 266 (2002).
[32] M. Yu. Romanovsky, Zh. Eksp. Teor. Fiz. **114**, 1230 (1998); [JETP **87**, 672 (1998)].
[33] S. A. Mayorov, A. N. Tkachev, and S. I. Yakovlenko, Usp. Fiz. Nauk **164**, 297 (1994); [Phys. Usp. **37**, 279 (1994)].
[34] S. G. Kuzmin and T. M. O'Neil, Phys. Rev. Lett. **88**, 065003 (2002).
[35] S. G. Kuzmin and T. M. O′Neil, Phys. Plasmas **9**, 3743 (2002).
[36] A. V. Lankin and G. E. Norman, Teplofiz. Vys. Temp. **46**, 170 (2008); High Temp. **46**, 148 (2008).
[37] A. V. Lankin, Zh. Eksp. Teor. Fiz. **134**, 1013 (2008); [JETP **107**, 870 (2008)].
[38] B. M. Smirnov, *Physics of Ionized Gases* (Wiley, New York, 2001).
[39] W. G. Graham, W. Fritsch, Y. Hahn, and J. A. Tanis, *Recombination of Atomic Ions*, NATO Advanced Studies Institute, Series B: Physics (Plenum, New York, 1992), Vol. 296.
[40] J. Abdallah, Jr., *et al.*, Phys. Rev. A **68**, 063201 (2003).
[41] B. Rethfeld, K. Sokolowski-Tinten, D. von der Linde, and S. I. Anisimov, Appl. Phys. A: Mater. Sci. Process. **79**, 767 (2004).
[42] N. A. Inogamov, A. M. Oparin, Yu. V. Petrov, N. V. Shaposhnikov, S. I. Anisimov, D. von der Linde, and J. Meyer-ter-Vehn, Pis'ma Zh. Eksp. Teor. Fiz. **69**, 284 (1999); [JETP Lett. **69**, 310 (1999)].
[43] A. Gokhman, J. Boemert, and A. Ulbricht, J. Nucl. Mater. **334**, 195 (2004).
[44] A. Gokhman and J. Bohmert, Radiat. Eff. Defects Solids **158**, 499 (2003).